Draft version March 8, 2013
Preprint typeset using LaTeX style emulateapj v. 5/2/11

arXiv:1206.5002v1 [astro-ph.GA] 21 Jun 2012

STELLAR WIND MASS RETENTION IN STAR CLUSTERS: IMPLICATIONS FOR SUBSEQUENT EPISODES OF STAR FORMATION

J.P. Naiman, E. Ramirez-Ruiz, D. N. C. Lin[1]

Draft version March 8, 2013

ABSTRACT

The discovery of multiple evolutionary sequences has challenged the paradigm that globular clusters (GCs) host simple stellar populations. In addition, spectroscopic studies of GCs show a spread in light-element abundances, suggesting that multiple sequences can be formed from gaseous ejecta processed in evolved cluster stars. If multiple sequences originate from within GCs, then it should be determined how such stellar systems retain gas, form new stars within them and subsequently evolve. Here we expand upon previous studies and carry out hydrodynamical simulations that explore a wide range of cluster masses, compactness, metallicities and stellar age combinations in order to determine the ideal conditions for gas retention. We find that up to 6.4% of the mass of the star cluster can be made up of retained stellar wind gas at the time star formation is triggered. However, we show that multiple episodes of star formation can take place during the lifetime of a star cluster in particular for times $\gtrsim 1$ Gyr, thus leading to a sizable enhancement in the total number of new stars. The fact that this favorable star formation time interval coincides with the asymptotic giant branch (AGB) phase seems to give further credence to the idea that, at least in some GCs, there are stars which have formed from material processed by a previous generation of stars. The ability of extended heating sources, such as pulsar outflows or accretion onto compact objects, to hamper gas retention is illustrated via a simple numerical treatment.

Subject headings: globular clusters:general, hydrodynamics, accretion

1. INTRODUCTION

The idea that stars in globular clusters (GCs) are a coeval population has been a long disputed topic with significant discussion devoted to the presence (or lack thereof) of multiple main sequences and subgiant branches (see Piotto 2009, for a review). However, recent observational evidence has demonstrated that these multiple stellar populations (MSPs) are not only ubiquitous but also make up a sizable fraction (∼40-60%) of the total stellar mass (Caloi & D'Antona 2007; D'Antona & Caloi 2008). Spectroscopic observations of MSPs in GCs have also unveiled differences in their light element abundances (see e.g. Gratton et al. 2004; de Silva et al. 2009; Martell & Smith 2009). These anomalies can only be produced if these MSPs were formed from material processed at temperatures $T > 10^7$K (D'Ercole et al. 2008; Renzini & Voli 1981; Ventura & D'Antona 2008b).

To explain the presence of MSPs with the observed abundance anomalies the following timeline has been identified (Conroy & Spergel 2011; Cottrell & Da Costa 1981; Smith 1987; Carretta et al. 2010b): after the first generation of stars is formed and intracluster gas is expelled by supernovae, matter processed in the interiors of AGB stars is returned to the ISM through winds and after several 100 Myrs a second generation of stars is formed from a mixture of stellar-processed material and captured ISM gas. Some of the issues at the forefront of attention include the type and age of stars able to process gas at the required internal temperatures while at the same time efficiently returning material into GCs to form a sizable mass fraction of new stars. We address both of these issues here.

The effective retention of stellar wind material to create MSPs of comparable mass presents a challenge to the current understanding of GC formation (Conroy 2011). Accounting for the inflow and mixing of pristine ISM material slightly lowers the retained mass requirements, however the original GCs still need to be significantly more massive than those currently observed (Naiman et al. 2011; Pflamm-Altenburg & Kroupa 2009; D'Ercole et al. 2010; Conroy & Spergel 2011). Despite their relevance, stellar wind gas retention has so far only been studied for a very restricted number of systems (D'Ercole et al. 2008, 2010; Conroy 2011; Conroy & Spergel 2011). Here we expand upon these studies with hydrodynamical simulations which explore the possible combinations of cluster mass, compactness and stellar age to determine the optimum parameter space for maximal gas retention.

2. NUMERICAL METHODS AND INITIAL SETUP

2.1. *Hydrodynamics*

To examine the ability of clusters to effectively retain the winds emanating from their evolving stellar members, we simulate mass and energy injection in isolated core potentials under the assumption of spherical symmetry (Quataert 2004; Hueyotl-Zahuantitla et al. 2010). The one-dimensional hydrodynamical equations are solved using FLASH, a parallel, adaptive mesh refinement hydrodynamical code (Fryxell et al. 2000). The winds from the closely packed stellar members are assumed to shock and thermalize such that density and energy contributions can be treated as source

---

[1] TASC, Department of Astronomy and Astrophysics, University of California, Santa Cruz, CA 95064

terms in the hydrodynamical equations. In spherical symmetry, these equations can be written as (Holzer & Axford 1970; Hueyotl-Zahuantitla et al. 2010):

$$\frac{\partial \rho}{\partial t} + \frac{1}{r^2}\frac{\partial}{\partial r}\left(\rho u r^2\right) = q_m(r) \tag{1}$$

$$\frac{\partial u}{\partial t} + u\frac{\partial u}{\partial r} + \frac{1}{\rho}\frac{\partial P}{\partial r} = -\frac{d\Phi_g}{dr} - q_m(r)u \tag{2}$$

$$\frac{\partial \varepsilon}{\partial t} + \frac{1}{r^2}\frac{\partial}{\partial r}\left(\varepsilon u r^2\right) + P\frac{\partial u}{\partial r} = q_\varepsilon(r) - Q(r) \tag{3}$$

where $P = P(r)$, $\rho = \rho(r)$, $u = u(r)$ and $\varepsilon = \varepsilon(r)$ are the gas density, pressure, radial velocity and internal energy density, respectively. Here, $Q(r) = n_i(r)n_e(r)\Lambda(T, Z)$ is the cooling rate for gas with ion and electron number densities $n_i(r)$ and $n_e(r)$, and $\Lambda(T, Z)$ is the cooling function for gas at temperature T and metallicity Z. We use $\Lambda(T, Z)$ from Gnat & Sternberg (2007) for $T > 10^4$ K and Dalgarno & McCray (1972) for $10 \leq T \leq 10^4$ K.

The $q_m(r)$ and $q_\varepsilon(r)$ terms in equations (1)-(3) are used here to mediate the total rate of mass and energy injection. For N stars each with average mass loss rate $\langle\dot{M}\rangle$ and wind energy injection rate $\frac{1}{2}\langle\dot{M}\rangle\langle v_w^2\rangle$ we have $\dot{M}_{\rm w,total} = N\langle\dot{M}\rangle = \int 4\pi r^2 q_m(r)dr$ and $\dot{E}_{\rm w,total} = \frac{1}{2}N\langle\dot{M}\rangle\langle v_{\rm w}^2\rangle = \int 4\pi r^2 q_\varepsilon(r)dr$, such that $q_\varepsilon(r) = \frac{1}{2}q_m(r)\langle v_{\rm w}^2\rangle$. For simplicity, we neglect the effects of mass segregation and assume $q_m(r) \propto n(r) \propto r^{-2}\frac{d}{dr}\left(r^2\frac{d\Phi_g}{dr}\right)$. We also neglect the effects of external mass accumulation, which can be an important source of gas when clusters reside in cool, dense ISM gas (Naiman et al. 2009, 2011). While specific heating sources such as photoionization or supernova are not explicitly included, the overall effects of additional energy injection in the cluster are discussed in §4.

The stellar cluster gravitational potentials are modeled as Plummer models (Brüns et al. 2009; Pflamm-Altenburg & Kroupa 2009)

$$\Phi_g = -\frac{GM_c}{\left[r^2 + r_c^2(\sigma_v)\right]^{1/2}} \tag{4}$$

for a given total mass, M_c, and velocity dispersion, $\sigma_v = \left(3^{3/4}/\sqrt{2}\right)^{-1}\sqrt{GM_c/r_c}$. In addition to following the dynamics of the gas under the influence of Φ_g, the self gravity of the gas is computed using FLASH's multipole gravity module.

In cases where catastrophic cooling occurs, a sub-grid model for star formation is implemented to prevent premature collapse. Our cooling prescription is modified following Truelove et al. (1997) by turning off energy losses and allowing the gas to evolve adiabatically when the Jean's length of the collapsing gas structure is comparable (or smaller than) to the cell size of our simulation. Such a method approximates the transition of an isothermally collapsing cloud to an optically thick, adiabatically evolving protostellar cluster while forgoing the computationally expensive three dimensional radiative transfer calculations required to treat this problem accurately. Because we do not include an explicit star formation prescription, we allow such unstable regions to evolve for a few sound crossing times before halting the simulation.

2.2. *Stellar Evolution*

To estimate the net mass loss and mean thermal velocities of the colliding winds, we first follow the formalism developed by Pooley & Rappaport (2006) where the integrated wind kinetic energy and mass loss of the stellar population's turn off star is used as a proxy for the average wind velocity and mass loss rate:

$$\langle v_{\rm w,to}^2\rangle \approx \frac{2\Delta E_K}{\Delta M} \tag{5}$$

$$\langle\dot{M}_{\rm to}\rangle \approx \frac{\Delta M}{\Delta t}. \tag{6}$$

Here $\Delta E_K = \frac{1}{2}\int_{t_1}^{t_2}\dot{M}_{\rm to}v_{\rm w,to}^2 dt$ and $\Delta M = \int_{t_1}^{t_2}\dot{M}_{\rm to}dt$ are the kinetic energy and mass loss input rates integrated over the lifetime of the turn-off stars, $\Delta t = t_2 - t_1$.

The effects of the additional input of mass and kinetic energy by stars with $M_\star < M_{\star,\rm to}$, which are neglected in the formalism we just outlined, can be included by convolving the above definitions of the average mass loss rate and wind velocity with an initial mass function (IMF) and a star formation history. Following Kroupa et al. (2011), the average number of stars in a mass interval $[M_\star, M_\star + dM_\star]$ evolving between $[t, t+dt]$ is given by $dN = \zeta(M_\star, t)b(t)dM_\star dt$ where $\zeta(M_\star, t)$ is the IMF, which we assume is accurately described by the Kroupa (2001) IMF, and $b(t)$ is the normalized star formation history. For a non-evolving IMF, $\zeta(M_\star, t) = \zeta(M_\star)$, with a mass distribution extending from $M_{\star,L}$ to $M_{\star,H}$, the normalized star formation history can be written as $\int_0^{t_{\rm age}(M_{\star,L})} b(t)dt = 1$, where $t_{\rm age}(M_\star)$ is the lifetime of a star of a given $M_\star$. Examples of $b(t)$ include a constant star formation rate, $b(t) = 1$, or a coeval population, $b(t) = \delta(t - t_0)$, with all stars formed at t_0.

The average mass $\langle\Delta M(t_i)\rangle$ and kinetic energy $\langle\Delta E_K(t_i)\rangle$ injected into the cluster environment at a time t_i, by a population of stars with $M_\star \epsilon\ [M_{\star,L}, M_{\star,H}]$ and whose birth rate is regulated by $b(t)$, are then given by

$$\langle\Delta M(t_i)\rangle = \int_{t_0}^{t_i} b(t) \int_{M_{\star,\mathrm{L}}}^{M_{\star,\mathrm{H}}} \zeta(M_\star)\dot{M}(M_\star,t)dM_\star dt \tag{7}$$

and

$$\langle\Delta E_K(t_i)\rangle = \frac{1}{2}\int_{t_0}^{t_i} b(t) \int_{M_{\star,\mathrm{L}}}^{M_{\star,\mathrm{H}}} \zeta(M_\star)\dot{M}(M_\star,t)v_w^2(M_\star,t)dM_\star dt, \tag{8}$$

respectively. Stars that have lifetimes $t_{\rm age}(M_\star) < t_i$ forsake the stellar population unless they were born during the most recent star formation time interval $[t_i - t_{\rm age}(M_\star), t_i]$. For this reason, t_0 is set to $\max[0, t_i - t_{\rm age}(M_\star)]$. This formalism allows for equations (5) and (6) to be cast into a more general form

$$\langle\dot{M}(t_i)\rangle = \frac{\langle\Delta M(t_i)\rangle}{t_i} = \frac{1}{t_i}\int_{t_0}^{t_i} b(t) \int_{M_{\star,\mathrm{i}}}^{M_{\star,\mathrm{f}}} \zeta(M_\star)\dot{M}(M_\star,t)dM_\star dt \tag{9}$$

and

$$\langle v_w^2(t_i)\rangle = \frac{2\langle\Delta E_K(t_i)\rangle}{\langle\Delta M(t_i)\rangle} = \langle\dot{M}(t_i)\rangle^{-1}\int_{t_0}^{t_i} b(t) \int_{M_{\star,\mathrm{i}}}^{M_{\star,\mathrm{f}}} \zeta(M_\star)\dot{M}(M_\star,t)v_w^2(M_\star,t)dM_\star dt. \tag{10}$$

In what follows, we assume the stellar population initially residing in star clusters is coeval such that $b(t) = \delta(0)$, which provides an accurate description for clusters with $t_i \gtrsim 10$ Myrs.

To compute the individual mass loss rates $\dot{M}(M_\star, t)$ and wind velocities $v_w(M_\star, t)$ we use the MESA stellar evolution models (Paxton et al. 2011). We use this code to follow the evolution of a grid of stellar models with $M_\star = 0.1\,M_\odot$ - $20\,M_\odot$ from ZAMS to either the white dwarf stage, end of the AGB phase, or compact object creation. The mass loss rates during the crucial AGB phase are estimated here using the wind prescription of Bloecker (1995) with a normalization of $\eta_B = 0.04$ consistent with LMC measurements (Ventura et al. 2000). We fix $Z = 1/10 Z_\odot$ for most models although the effects of changing the metallicity are discussed in §4.

3. STELLAR WIND RETENTION IN STAR CLUSTERS

The mass injection properties, characterized here by the mass loss rates and wind velocities emanating from a coeval population of stars, change dramatically as the population evolves. Figure 1 shows the evolution of the average stellar wind parameters. As the wind velocities and stellar mass loss rates change, so does the ability of a cluster potential to retain the shocked stellar wind gas. Note that the differences between the turn off mass and population averaged prescriptions manifests itself predominately in the values of the wind velocity.

A young star cluster, corresponding to time A in Figure 1, with its high average wind velocity cannot retain gas effectively if $\sigma_v \ll v_w$. This is clearly seen in Figure 2 which shows the properties of the shocked stellar wind gas confined to a cluster potential characterized by $\sigma_v = 50\,\mathrm{km/s}$ and $M_c = 10^7\,M_\odot$ for both turn off mass and population averaged prescriptions (*red* curves). The flow in this case was evolved for $t_i = t_A$. A young cluster is thus only likely to retain a small quantity of high temperature gas in its inner region, while further away gas is blown out of the system in a wind. As the cluster members evolve, a dramatic decrease in the average wind velocity occurs due to the dominant contribution of the slow, dense AGB winds to the overall mass injection, corresponding to time B in Figure 1. For the star cluster, here assumed to be characterized by a non-evolving gravitational potential, the AGB contribution results in stellar wind injection parameters that favor significant mass retention, as shown in Figure 1 (*black* curves). As the stellar wind gas shocks and cools, mass is efficiently accumulated until the central region becomes Jeans unstable, thus triggering star formation. In this case, the gas flow within the cluster is evolved until $t = t_{\rm sf}$, defined here as the sound crossing time within the (adequately resolved) Jeans unstable region. As the cluster ages, remaining stars no longer pass through an extended thermally pulsing AGB phase. This results in a dramatic increase in average wind velocity and decrease in average mass loss rates as seen at time C. As a result, the cluster potential is unable to effectively retain the emanating gas and the wind material flows out of the cluster almost unrestrained.

The ability for a star cluster to retain wind ejecta depends not only on the evolutionary stage of its members but also on their spatial distribution. To illustrate this, in Figure 3 we show the properties of the shocked stellar wind gas confined to a shallow potential characterized by $\sigma_v = 14\,\mathrm{km/s}$ and $M_c = 4.5 \times 10^5\,M_\odot$, parameters thought to accurately represent the current stellar mass distribution in M15 (McNamara et al. 2004; Gerssen et al. 2002). A shallow gravitational potential is thus unable to retain a significant amount of stellar wind material, even during the AGB phase. The observational constraint on the allowed gas density in M15 (Knapp et al. 1996) is consistent with our predictions for the present state of the gas in this system.

The dramatic difference observed in Figures 2 and 3 between the stellar wind mass accumulated in cluster potentials of varying properties motivates our study to compare results obtained with different velocity dispersions and cluster masses. To facilitate comparisons, we first systematically vary the cluster velocity dispersion for a fixed total mass $M_c = 10^7\,M_\odot$, assuming the turn off mass wind velocity and mass loss rate are representative of the entire population. The left panel of Figure 4 gives the amount of accumulated stellar wind mass in units of M_c for a range of cluster velocity dispersions and different evolutionary stages (t_i) of the stellar members. By looking at the shaded regions in Figure 4, the reader can identify the cluster velocity dispersion and mass combinations for which favorable conditions for star formation are satisfied at a given cluster age.

Cluster potentials with $\sigma_v \lesssim 20\,\mathrm{km/s}$ are not effective at retaining gas in their cores, and gas is blown out of the cluster at all times. As the velocity dispersion increases above $30\,\mathrm{km/s}$, the cluster core is able to retain the shocked and efficiently cooled stellar wind gas, making the central region Jeans unstable before (i.e. $t_{\mathrm{sf}} \ll t_i$) a significant amount of mass is accumulated into the cluster. The largest fraction of mass retained takes place for star clusters with $\sigma_v \approx 25\,\mathrm{km/s}$. In this case, the potential is steep enough to retain the shocked and subsequently cooled wind material, but shallow enough to force the cold gas to collapse only until a significant amount of mass has been accumulated. The contours in the left panel of Figure 4 show that potentials with $\sigma_v \gtrsim 30\,\mathrm{km/s}$ can endure multiple episodes of star formation albeit involving less retained gas, while potentials with $25\,\mathrm{km/s} \lesssim \sigma_v < 30\,\mathrm{km/s}$ can have only short but more intense star formation periods. The largest mass accumulation for a single star formation episode occurs for $\sigma_v \approx 27\,\mathrm{km/s}$ between the ages of $1-10$ Gyrs, with a mass retention fraction of $M_{\mathrm{acc}}/M_c \approx 6.4\%$. This value is lower than the ≈10% estimated by previous studies (Conroy 2011; D'Ercole et al. 2008), owing to the fact that we used the time averaged values of the wind velocity which results in about five times larger kinetic energy injection rates than using the instantaneous values.

The right panel of Figure 4, in conjunction with the left panel, allows us to estimate the amount of stellar wind material retained by a star cluster of a given age, mass and velocity dispersion. The conclusions drawn are based upon the assumption that the cluster potential properties, whose evolution causes are poorly known, remain relatively unaltered for $\min[t_i, t_{\mathrm{sf}}]$. The right panel of Figure 4 is self-explanatory - heavier star clusters at a fixed velocity dispersion retain more gas. The mass retention fraction is observed to increase slightly with augmenting cluster mass as a result of less efficient cooling, which in turn delays the triggering of star formation as mass continues to accumulate.

Using the average wind velocity and mass loss rate of the turn off mass star to represent the properties of the entire population underestimates the kinetic energy input arising from the more numerous, lighter stars (Figure 1). This gives an optimistic value of the wind retention and star formation efficiencies. The effects of using the total kinetic energy input from the star cluster to calculate effective mass retention are shown in Figure 5. Direct comparison with Figure 4 shows that although the overall mass accumulation is rather similar, in the population-averaged prescription star formation is triggered over a narrower range of velocity dispersions. Not only are higher velocity dispersions required to produce efficient star forming models, but the additional kinetic energy inhibits star formation in the largest mass accumulation regions. This is because the larger wind velocities keep the gas at higher temperatures, thus quenching star formation. This mass is subsequently blown out of the cluster at later times when the mass loss rates decrease and the accompanying wind velocities increase. These results clearly indicate that care must be taken when attempting to estimate the amount of new stars that can be subsequently formed in star clusters as this strongly depends on the assumed mass loss prescriptions, which are uncertain.

While the assumed wind prescription can alter the total amount of gas retained which can create new stars, the contours in Figures 4 and 5 suggest that a stellar cluster with favorable potential parameters, $[M_c, \sigma_v]$, can trigger star formation over a large span of time. In reality, an episode of star formation will trigger subsequent supernova outbursts which can drive gas away from the central regions of the cluster, deterring further star formation. We simulate the effects of supernova explosions on gas retention by adding thermal energy to the central region of a typical cluster once star formation has been triggered. To maximize the effects of feedback in our cluster, we assume a **large** star formation efficiency of 90%, creating $M_\star \approx 10^6\,M_\odot$ in second generation stars for a model from the left panel of Figure 4 with a 6.4% retention rate. Following the method of D'Ercole et al. (2008), we add in $E_{SN} = 10^{51}\,\mathrm{ergss}^{-1}$ in the central regions of our simulation at a rate of $2\times10^{-6}\mathrm{yr}^{-1}$. This has been scaled from their supernova type Ia rate of $2\times10^{-5}\,\mathrm{yr}^{-1}$ for a $M_c = 10^7\,M_\odot$ population (Marcolini et al. 2006). After a period of 100 Myrs the supernova energy injection is halted and the gas is once again allowed accumulate in the central regions of the cluster, starting the cycle over. Figure 6 shows this cycle of mass accumulation, star formation and supernova feedback for a simulation at $t_{age} \approx 2000\,\mathrm{Myrs}$ for a model with $M_c = 10^7\,M_\odot$, $\sigma_v = 26\,\mathrm{km/s}$, and $M_{\mathrm{acc}}/M_{\mathrm{c}} = 6.4\%$. Here, it takes approximately 2000 Myrs for the cluster to re-trigger star formation once gas has been removed by 100 Myrs of type Ia supernova feedback.

4. DISCUSSION

Throughout this work, we have used simplified models to determine how effective a star cluster of a particular age is at retaining gas emanating from its stellar members, under the assumption that its potential remains unaltered during the simulated phase. We have further assumed a single metallicity for all clusters and have disregarded any heating sources besides supernova feedback and the stellar winds themselves. In this section we relax both of these assumptions.

4.1. *Metallicity*

Cluster to cluster variations in light element abundances are commonly observed (Caldwell et al. 2011; Beasley et al. 2005). These variations may cause changes in the mass loss histories of the individual stellar members and the cooling properties of the shocked gas. As the stellar mass loss prescription are mostly independent of metallicity during the evolutionary time periods that are conducive to star formation ($0.1\,\mathrm{Gyrs} \lesssim t_i \lesssim 100\,\mathrm{Gyrs}$) (Bloecker 1995), we account for the effects of varying metallicity solely in the cooling function. Figure 4 shows the effects of changing metallicity for a typical star forming cluster, described here by $M_c = 10^7\,M_\odot$, $\sigma_v = 50\,\mathrm{km/s}$, and $t_i = 212\,\mathrm{Myrs}$. As the metallicity is decreased, the cooling becomes less efficient and more material is allowed to flow into the center of the cluster before catastrophic cooling occurs. This enables relatively more massive star forming episodes to be triggered. Interestingly, when metallicity is decreased beyond $Z < 10^{-1}$, the cooling becomes weak enough to prevent catastrophic cooling at times $\leq t_i$. These results suggest that the range of cluster parameters over which large central densities will persist before catastrophic cooling takes place (Figure 4) will depend on the metallicity of the emanating stellar winds, though, as illustrated in Figure 7, the differences are not marked.

4.2. *Intercluster Heating Sources*

In addition to altering the cooling curves, the inclusion of additional cluster heating sources may prevent effective gas retention in our simulations. We address this problem here by artificially increasing the energy input rate: $q_{\epsilon,\mathrm{new}} = (1+H)q_\epsilon = (1+H)\frac{1}{2}q_m(r)v_w^2$. Under this assumption, the additional heating sources follow the potential's stellar distribution. Figure 8 shows the effects of the additional heat input in one of our otherwise star forming simulations. For $H < 2.0$, the gas in the simulation still collapses, triggering star formation. For larger values, on the other hand, the cluster is unable to effectively retain the gas and, as a result, star formation never ensues. By integrating $q_{\epsilon,\mathrm{new}}$ over the cluster's core for $H = 2.0$, we derive the total energy input rate required to overturn the central mass build up, which for this simulation is about $10^{35}\,\mathrm{ergs}^{-1}$.

In many cases, the additional energy injection sources might not follow the stellar distribution. As an example, let's compare the heat distribution expected from accreting neutron stars under the assumption that the accretion feedback is proportional to the Bondi accretion rate: $q_{\epsilon,\mathrm{ns}} \propto \dot{M} \propto \rho(r)T(r)^{-3/2}$ (Bondi & Hoyle 1944). Using the volume-averaged density and temperature in the cluster core, $\bar{\rho} \approx 10^{-22}\,\mathrm{g\,cm}^{-3}$ and $\bar{T} \approx 10^4$K, we derive the average luminosity of a single, accreting neutron star: $L_{NS} \approx 10^{33}\,\mathrm{ergs\,s}^{-1}$. This implies that $\gtrsim 100$ accreting neutron stars are required to reside in the cluster's core in order to significantly offset its cooling properties. However, to accurately test this phenomena a multi-dimensional approach would be required as feedback would not necessarily act as a simple heating prescription.

In this work, we have also tried to minimize the effect of external mass inflow by considering star clusters in isolation. This is certainly not the case for clusters moving through cold, dense environments, as they can potentially amass a significant amount of gas from their surroundings (Naiman et al. 2009, 2011). The stellar winds and exterior inflows in such clusters could combine to create even larger central density enhancements (Naiman et al. 2009, 2011; Conroy & Spergel 2011; Priestley et al. 2011; Pflamm-Altenburg & Kroupa 2009). A self consistent treatment of both interior and exterior gas accumulation in multi-dimensional simulations, which includes the effects of compact object accretion, tidal stripping, photoionization, and pulsar heating will be presented elsewhere.

While previous work has estimated the ability of star clusters to retain stellar winds (D'Ercole et al. 2008, 2010; Conroy 2011; Conroy & Spergel 2011), calculations have so far been restricted to a small range of cluster properties and stellar ages. Motivated by this, we have calculated gas retention in star clusters of various ages, stellar mass and compactness. In agreement with previous studies we find that before star formation is triggered about ≤10% of the total cluster mass is comprised of retained stellar wind gas, naively implying that the original proto-GCs had to be more massive than what is observed today (Conroy 2011; D'Ercole et al. 2008). However, we show that multiple episodes of star formation can in fact take place during the lifetime of a cluster in particular between ~ 1 and ~ 10 Gyrs, thus suggesting a sizable enhancement in star formation. The overlap of this time range with the AGB phase further strengthens the case for stellar wind retention as a critical component in the formation of subsequent generations of stars in GCs.

We thank Mark Krumholz, Charlie Conroy, David Pooley, Rebecca Bernstein, Chung-Pei Ma and Morgan Macleod for useful discussions. The software used in this work was in part developed by the DOE-supported ASCI/Alliance Center for Astrophysical Thermonuclear Flashes at the University of Chicago. Computations were performed on the Pleaides UCSC computer cluster. This work is supported by NSF: AST-0847563 (J.N. and E.R.), NASA: NNX08AL41G (J.N. and D.L.), and The David and Lucile Packard Foundation (E.R.).

REFERENCES

Beasley, M. A., Brodie, J. P., Strader, J., et al. 2005, AJ, 129, 1412
Bedin, L. R., Piotto, G., Anderson, J., et al. 2004, ApJ, 605, L125
Bloecker, T. 1995, A&A, 297, 727
Bondi, H., & Hoyle, F. 1944, MNRAS, 104, 273
Brüns, R. C., Kroupa, P., & Fellhauer, M. 2009, ApJ, 702, 1268
Caldwell, N., Schiavon, R., Morrison, H., Rose, J. A., & Harding, P. 2011, AJ, 141, 61
Caloi, V., & D'Antona, F. 2007, A&A, 463, 949
Carretta, E., Bragaglia, A., Gratton, R. G., et al. 2010, A&A, 516, A55
Conroy, C. 2011, arXiv:1101.2208
Conroy, C., & Spergel, D. N. 2011, ApJ, 726, 36
Cottrell, P. L., & Da Costa, G. S. 1981, ApJ, 245, L79
Dalgarno, A., & McCray, R. A. 1972, ARA&A, 10, 375
D'Antona, F., Bellazzini, M., Caloi, V., et al. 2005, ApJ, 631, 868
D'Antona, F., & Caloi, V. 2008, MNRAS, 390, 693
Decressin, T., Meynet, G., Charbonnel, C., Prantzos, N., & Ekström, S. 2007, A&A, 464, 1029
Decressin, T., Charbonnel, C., & Meynet, G. 2007, A&A, 475, 859
D'Ercole, A., D'Antona, F., Ventura, P., Vesperini, E., & McMillan, S. L. W. 2010, MNRAS, 407, 854
D'Ercole, A., Vesperini, E., D'Antona, F., McMillan, S. L. W., & Recchi, S. 2008, MNRAS, 391, 825
de Silva, G. M., Gibson, B. K., Lattanzio, J., & Asplund, M. 2009, A&A, 500, L25
Fryxell, B., et al. 2000, ApJS, 131, 273
Gerssen, J., van der Marel, R. P., Gebhardt, K., et al. 2002, AJ, 124, 3270
Gnat, O., & Sternberg, A. 2007, ApJS, 168, 213
Gratton, R., Sneden, C., & Carretta, E. 2004, ARA&A, 42, 385
Holzer, T. E., & Axford, W. I. 1970, ARA&A, 8, 31
Hueyotl-Zahuantitla, F., Tenorio-Tagle, G., Wünsch, R., Silich, S., & Palouš, J. 2010, ApJ, 716, 324

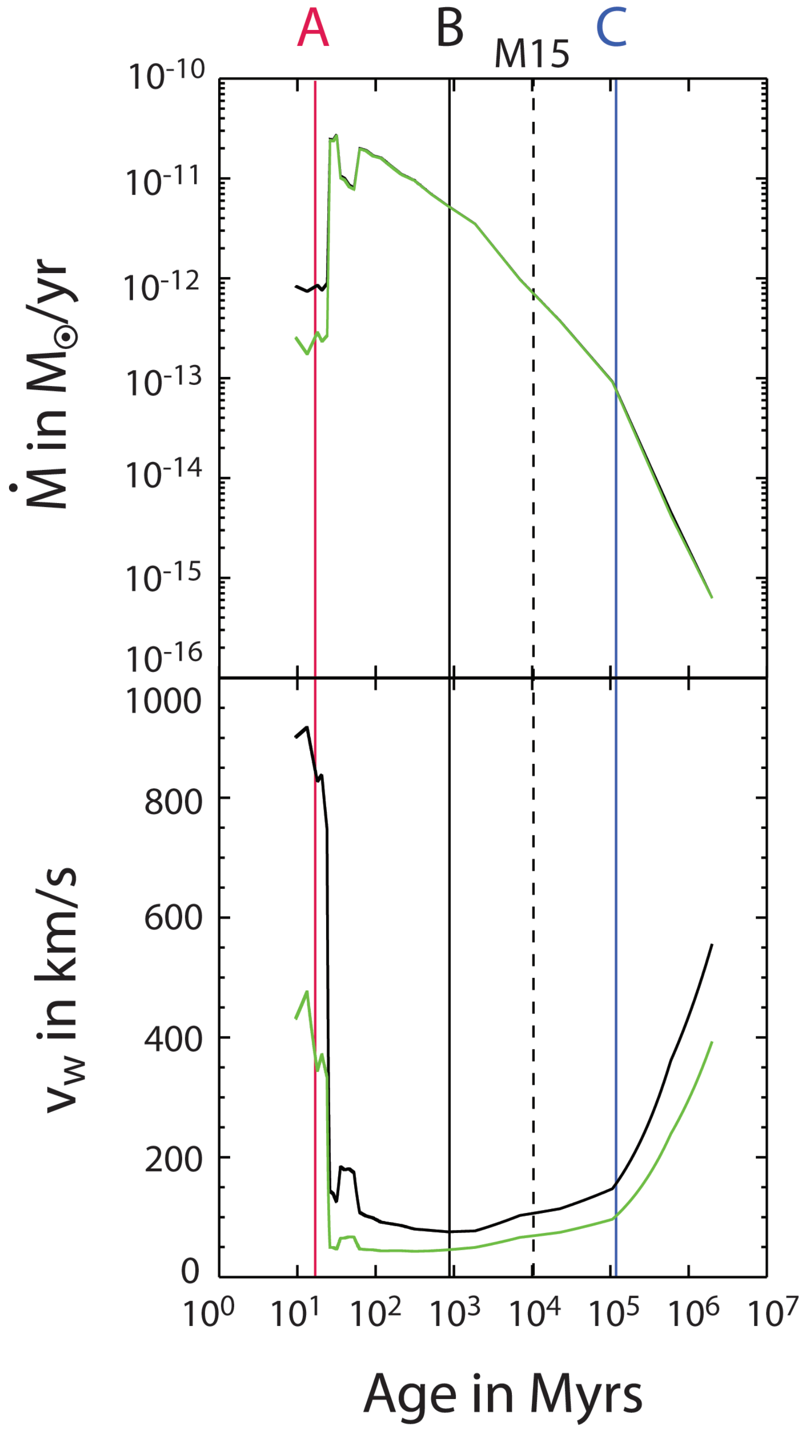

FIG. 1.— Average cluster mass loss rates and wind velocities as a function of time for $Z = 1/10Z_\odot$. Green lines assume gas dynamics are dominated by the wind properties of the turn off stars, black lines show the population averaged values. Three representative times in the clusters age are denoted by the solid vertical lines. The current age of M15 is denoted by the vertical dashed line.

Knapp, G. R., Gunn, J. E., Bowers, P. F., & Vasquez Poritz, J. F. 1996, ApJ, 462, 231
Kroupa, P. 2001, MNRAS, 322, 231
Kroupa, P., Weidner, C., Pflamm-Altenburg, J., et al. 2011, arXiv:1112.3340
Maeder, A., & Meynet, G. 2006, A&A, 448, L37
Marcolini, A., D'Ercole, A., Brighenti, F., & Recchi, S. 2006, MNRAS, 371, 643
Martell, S. L., & Smith, G. H. 2009, PASP, 121, 577
McNamara, B. J., Harrison, T. E., & Baumgardt, H. 2004, ApJ, 602, 264
Naiman, J. P., Ramirez-Ruiz, E., & Lin, D. N. C. 2009, ApJ, 705, L153
Naiman, J. P., Ramirez-Ruiz, E., & Lin, D. N. C. 2011, ApJ, 735, 25
Norris, J. E. 2004, ApJ, 612, L25
Paxton, B., Bildsten, L., Dotter, A., Herwig, F., Lesaffre, P., & Timmes, F. 2011, ApJS, 192, 3
Pflamm-Altenburg, J., & Kroupa, P. 2009, MNRAS, 397, 488
Piotto, G., Villanova, S., Bedin, L. R., et al. 2005, ApJ, 621, 777
Piotto, G., Bedin, L. R., Anderson, J., et al. 2007, ApJ, 661, L53
Piotto, G. 2009, IAU Symposium, 258, 233

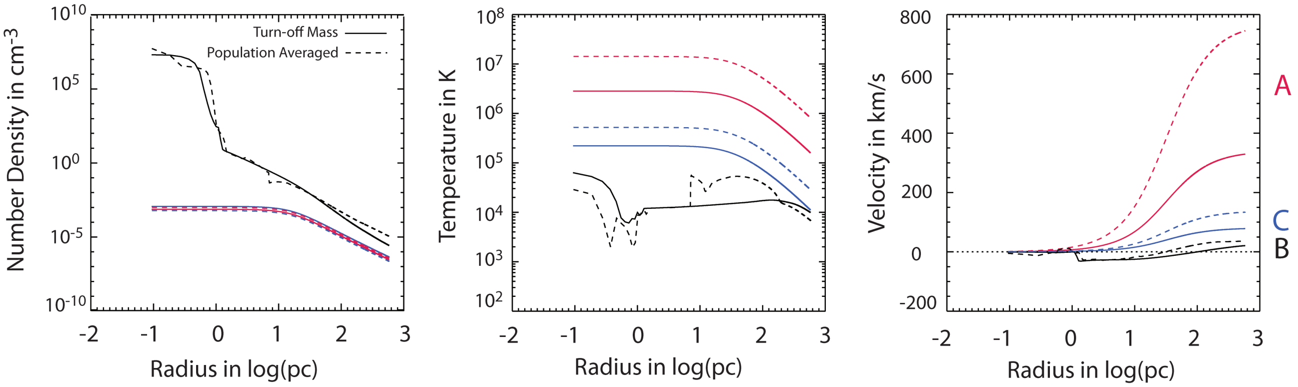

FIG. 2.— Hydrodynamic profiles for the three representative times denoted in Figure 1. These three plots are the density, temperature and velocity profiles at three representative times for a $M_c = 10^7\,M_\odot$, $\sigma_v = 30\,\mathrm{km/s}$ model. Solid and dashed lines represent the turn off mass and population averaged prescriptions, respectively.

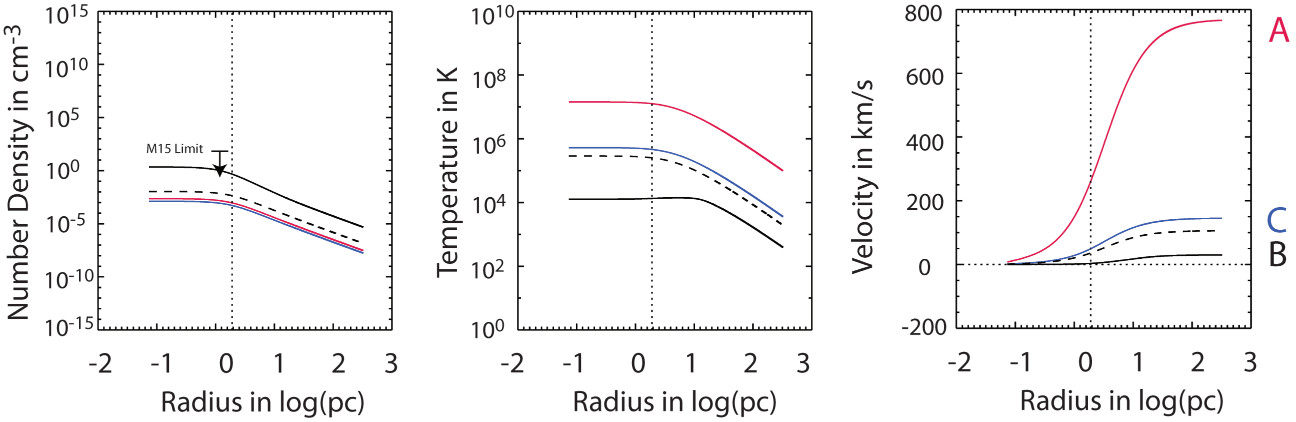

FIG. 3.— Hydrodynamic profiles for M15 with $M_c = 4.5 \times 10^5\,M_\odot$ and $\sigma_v = 14\,km/s$ (McNamara et al. 2004; Gerssen et al. 2002) at the three representative times in Figure 1, including the predicted profiles for its current age (dashed lines). Here, the population averaged prescription is used.

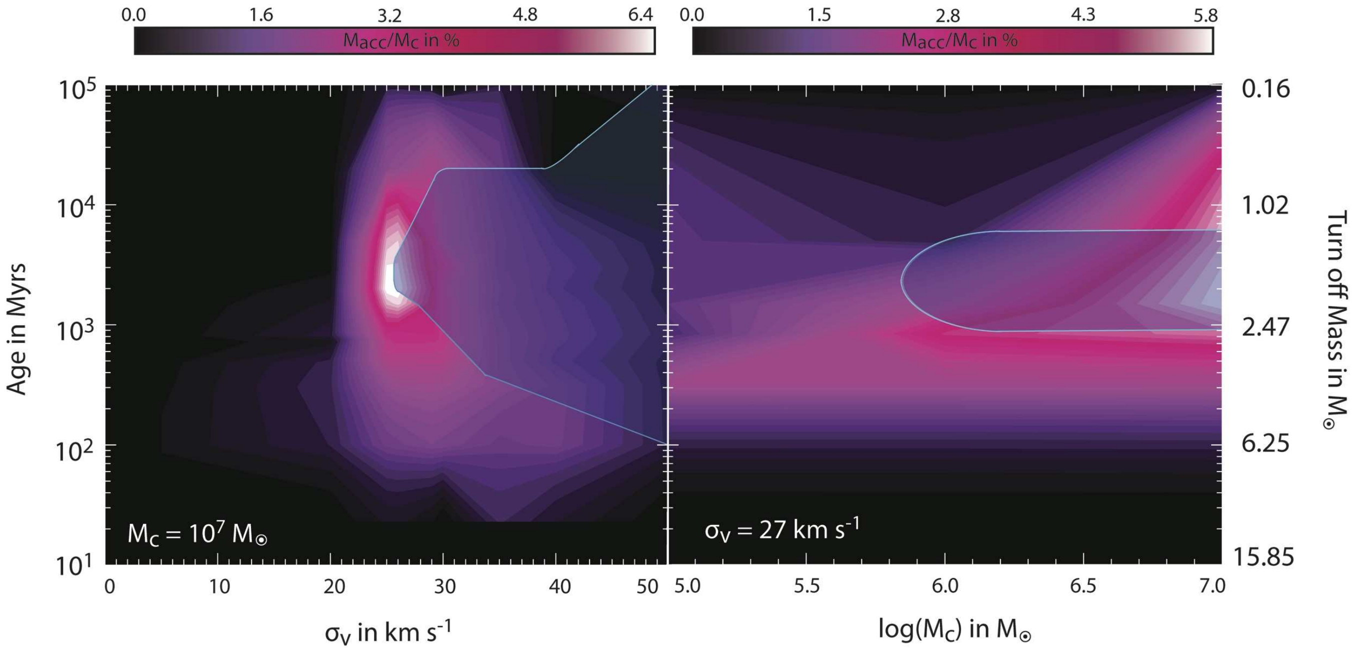

FIG. 4.— Mass accumulation, M_{acc}, as a function of the potential parameters M_{c} and σ for the turn off mass prescription. The blue shaded regions delimit the boundaries for which our models collapse and trigger star formation. *Right:* Contours of $M_{\mathrm{acc}}/M_{\mathrm{c}}$ for a fixed cluster core mass of $M_{\mathrm{c}} = 10^7\,M_\odot$ and a varying velocity dispersion. *Left:* Contours of $M_{\mathrm{acc}}/M_{\mathrm{c}}$ for a fixed velocity dispersion of $\sigma_v = 27\,\mathrm{km/s}$ and varying cluster mass.

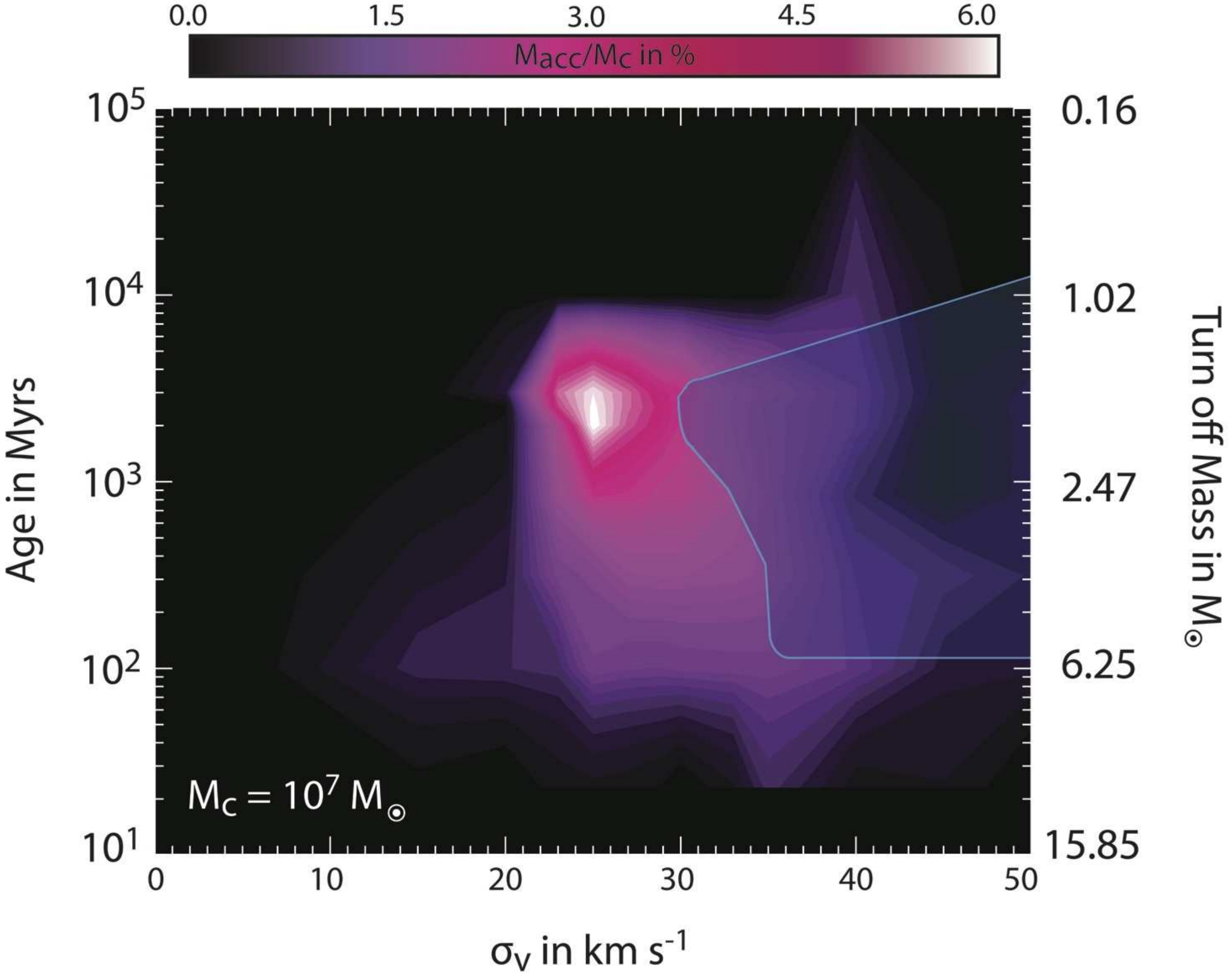

FIG. 5.— Mass accumulation, $M_{\rm acc}$, as a function of σ for a fixed cluster core mass of $M_{\rm c} = 10^7\,M_\odot$, calculated using the population averaged prescription. The blue shaded region delimits the boundaries for which our models collapse and trigger star formation.

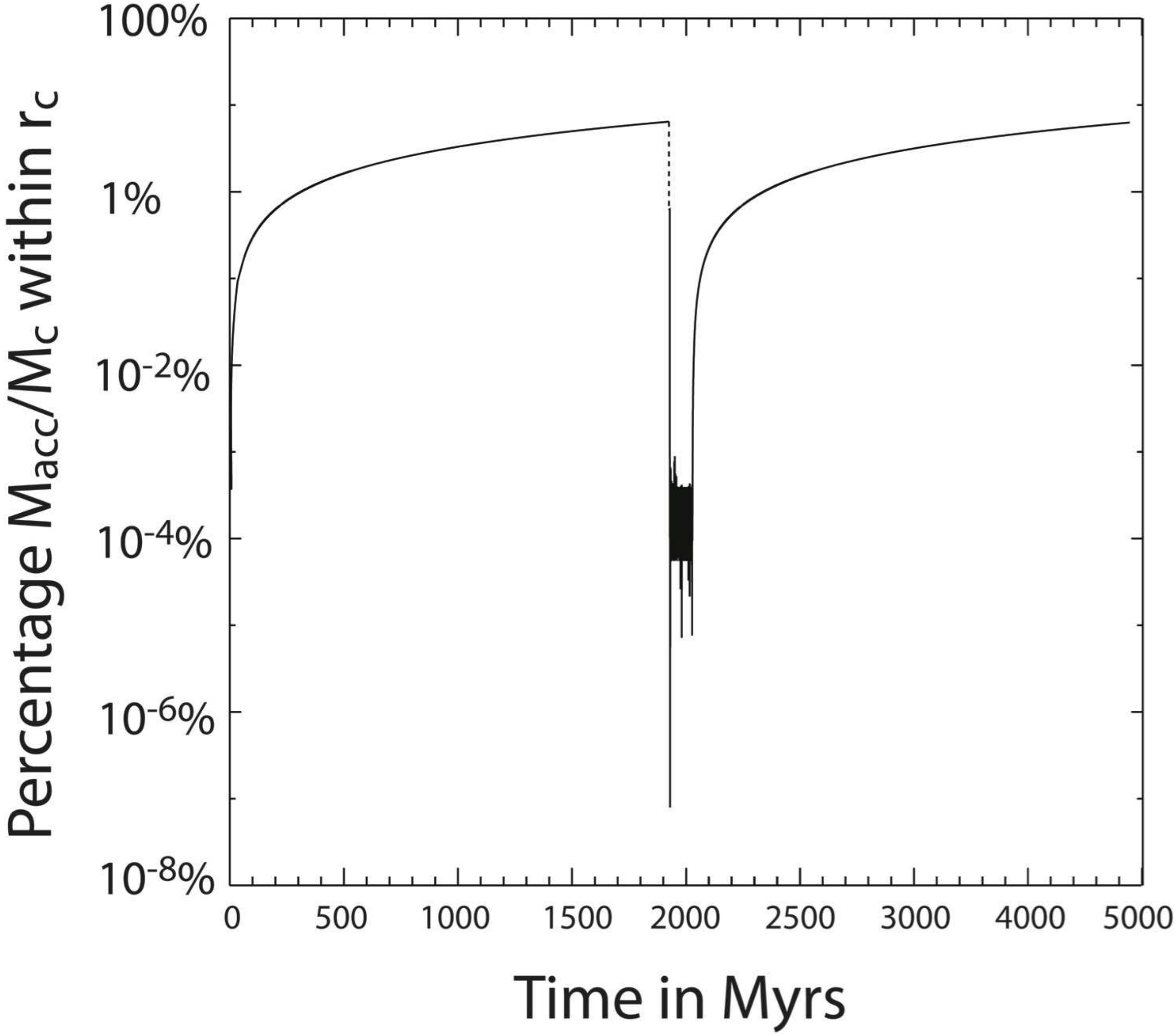

FIG. 6.— Cycles of mass accumulation in a potential with $M_c = 10^7\,M_\odot$, $\sigma_v = 26\,\mathrm{km/s}$ and $t_i = 2000\,\mathrm{Myrs}$ including star formation, and supernovae explosions. Mass accumulates till star formation is triggered, then 90% of this mass is assumed to form stars, removing the gas from the simulation (dashed lines). Supernovae persist for 100 Myrs at a rate of $2 \times 10^{-6}\,\mathrm{yr}^{-1}$ further stripping mass from the system. For simplicity, we have assumed the mass injection properties to be steady during the simulation.

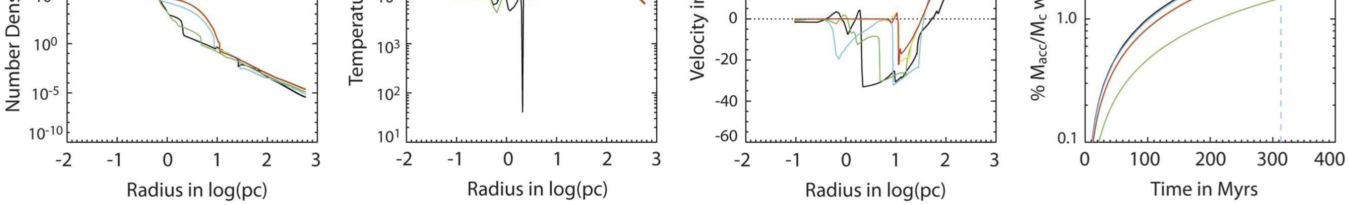

FIG. 7.— Gas properties for $M_c = 10^7\,M_\odot$, $\sigma_v = 30\,\mathrm{km/s}$ cluster at $t_i = 313\,\mathrm{Myrs}$ for different metallicities. Here, the population averaged values of the wind parameters are used.

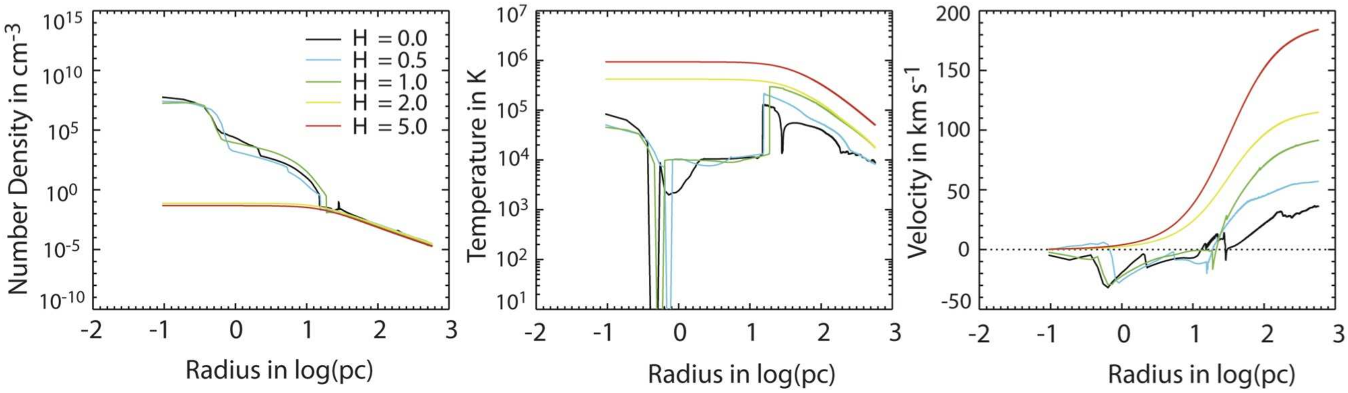

FIG. 8.— *Left 3 Plots:* Gas properties for $M_c = 10^7\,M_\odot$, $\sigma_v = 30\,\mathrm{km/s}$ cluster at $t_i = 1860$ Myrs with added heat in the form of thermal energy: $e_{int,new} = (1 + H)e_{int,old}$. Here, the population averaged values of the wind parameters are used.

Pooley, D., & Rappaport, S. 2006, ApJ, 644, L45
Prantzos, N., & Charbonnel, C. 2006, A&A, 458, 135
Priestley, W., Ruffert, M., & Salaris, M. 2011, MNRAS, 411, 1935
Quataert, E. 2004, ApJ, 613, 322
Renzini, A., & Voli, M. 1981, A&A, 94, 175
Smith, G. H. 1987, PASP, 99, 67
Truelove, J. K., Klein, R. I., McKee, C. F., Holliman, J. H., II, Howell, L. H., & Greenough, J. A. 1997, ApJ, 489, L179
Ventura, P., D'Antona, F., & Mazzitelli, I. 2000, A&A, 363, 605
Ventura, P., & D'Antona, F. 2008, A&A, 479, 805
Villanova, S., Piotto, G., King, I. R., et al. 2007, ApJ, 663, 296